Article:

Russell, J., Owen, J. and Hajirasouliha, I. orcid.org/0000-0003-2597-8200 (2018) Nonlinear behaviour of reinforced concrete flat slabs after a column loss event. Advances in Structural Engineering, 21 (14). pp. 2169-2183. ISSN 1369-4332

https://doi.org/10.1177/1369433218768968

Journal Title
XX(X):2–30

DOI: 10.1177/ToBeAssigned
www.sagepub.com/
SAGE

1

Nonlinear behaviour of reinforced concrete flat slabs after a column loss event

2 **J.M. Russell[1], J.S. Owen[2] and I. Hajirasouliha[3]**

Abstract

3 Previous studies have demonstrated that reinforced concrete flat slab structures could be vulnerable to progressive collapse. Although such events are highly dynamic, simplified static analyses using the sudden column loss scenario are often used to gain an indication into the robustness of the structure. In this study, finite element analysis is used to replicate column loss scenarios on a range of RC flat slab floor models. The model was firstly validated against the results of scaled slab experiments and then used to investigate the influence of different geometric and material variables, within standard design ranges, on the response of the structure. The results demonstrate that slab elements are able to effectively redistribute loading after a column loss event, and therefore prevent a progressive collapse. However, the shear forces to remaining columns were 159% of their fully supported condition and increased to 300% when a dynamic amplification factor of 2.0 was applied. It is shown that this can potentially lead to a punching shear failure in some of the slab elements.

Keywords

4 Progressive Collapse, Column Loss, RC Flat Slab, Punching Shear

Introduction

Since the collapse of Ronan Point tower building in 1968 the issue of progressive collapse of structures has been an important consideration for structural engineers. Much research has been aimed at understanding the response of different structural systems to a damaging event, commonly using the sudden column loss scenario. Extensive studies have covered the experimental, theoretical and numerical analysis of steel and Reinforced Concrete (RC) frame structures (Sasani et al. 2007; Flint et al. 2007; Yi et al. 2008; Su et al. 2009; Valipour and Foster 2010; Qian and Li 2013; Pham and Tan 2017). However the nature of flat slab construction creates a different response to extreme events compared to beam structures as a slab is able to redistribute forces more effectively. Previous events have demonstrated that flat slabs can be susceptible to progressive collapse, as seen with the Piper's Row car park, UK, in 1998 (Whittle 2013) or Sampoon department store, South Korea, 1995 (Gardner et al. 2002; Park 2012). RC Slabs can undergo brittle failure due to punching shear or exhibit geometric nonlinearity in the form of tensile or compressive membranes (Hawkins and Mitchell 1979; Mitchell and Cook 1984; Muttoni 2008; Qian and Li 2012; Dat and Hai 2013; Keyvani et al. 2014).

Finite Element (FE) analysis has been used successfully to model the response of structures to extreme events such as column loss, typically for framed structures (Kokot et al. 2012; Fu 2010; Kwasniewski 2010) and has been shown to suitably consider the nonlinear aspects involved. FE analysis has also been successfully used for RC slab sections (Trivedi and Singh 2013; Li and Hao 2013), including consideration of shear capacity (Mamede et al. 2013). However, accurate modelling of the post-punching behaviour remains a challenge for FE packages despite the work of others (Faria et al. 2012; Ruiz et al. 2013; Mirzaei and Sasani 2013; Genikomsou and Polak 2015).

[1]School of Engineering, University of Warwick, Coventry, UK
[2]Faculty of Engineering, The University of Nottingham, UK
[3]Department of Civil and Structural Engineering, The University of Sheffield, UK

Corresponding author:
Justin Russell, School of Engineering, University of Warwick, Coventry, UK
Email: j.russell.3@warwick.ac.uk

Furthermore, after Liu et al. (2015)'s important work into the response of flat slab structures to progressive collapse highlights that such structures can be highly susceptible to extreme events and that further studies are needed. As the potential for progressive collapse is dependant on the whole structural response it is important to consider the behaviour of a full floor section to consider the complete performance and what factors influence it. In particular the extent of damage and the potential for punching shear failure should be addressed.

This study therefore investigated the effect of column loss on a large RC flat slab floor structure. The main objectives are to demonstrate how the loading is redistributed, determine the extent of damage this causes, identify the potential overloading of surrounding columns and consider how geometric and material variations affect this. An FE model of a flat slab structure was validated against a series of experimental tests on scaled substructures and then a static push down analysis was conducted focusing on the nonlinear behaviour and the redistribution of forces after a column loss. The Critical Shear Crack Theory (CSCT) was applied to the surrounding columns to determine which areas and conditions might be susceptible to punching shear and would therefore require more detailed consideration.

Description of FE model

To assess the response of a concrete flat slab structure to column loss event, a FE model was created and analysed using Abaqus/Explicit (Simulia 2010). Solid, 8 node, brick elements (C3N8R) with reduced integration were used to model the concrete sections. Geometric non-linearities, for example compressive membrane action, are also taken into account by using such an approach. The nonlinear behaviour of the concrete was defined using the Concrete Damaged Plasticity (CDP) model suggested by Lubliner et al. (1989) and modified by Lee and Fenves (1998) which is based on a Drucker-Prager hyperbolic function. This damage model considers the behaviour of the concrete after cracking as a region of plastic strain, in effect representing a continuum of micro-cracks. This model has been regularly used for considering damage to concrete sections (Cicekli et al. 2007; Genikomsou and Polak 2015) due to its general purpose application for static and dynamic modelling of concrete. Full details can be found in the Abaqus manual (Simulia 2010). The uniaxial stress-strain behaviour of concrete in compression, after the linear elastic phase, is modelled with Equation 1 from CEB-fib du Béton (2012):

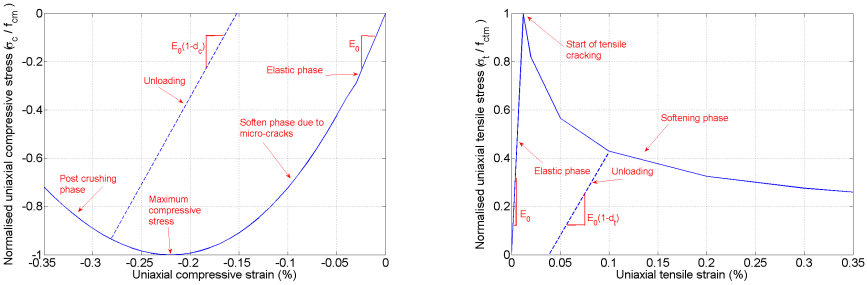

(a) Uniaxial compression (b) Uniaxial tension

Figure 1. Annotated concrete stress-strain models

$$\sigma_c = -f_{cm}\left(\frac{k\cdot\eta-\eta^2}{1+(k-2)\cdot\eta}\right) \tag{1}$$

where $\eta = \epsilon_c/\epsilon_{c1}$, i.e. the ratio of compression strain to crushing strain, and k is the plasticity number taken as 2.15 for C25/30 concrete. This gives a parabola shape beyond the elastic limit (see Figure 1(a)), with a softening effect until the ultimate limit, f_{cm}, due to compressive micro-cracks. After this point, there is a reduction in capacity as the concrete crushes. However, from all the scenarios considered with this FE model, only in the most extreme cases was the compression ultimate limit exceeded and so the material definition for this range is not believed to be critical to the results.

In tension, concrete is taken to be linear elastic up to its cracking stress, after which a nonlinear tension softening model is used to account for the reduction in the capacity of concrete. This is described Figure 1(b) according to Okamura and Maekawa (1990).

$$\sigma_t = \begin{cases} E_0\cdot\epsilon_t & for \quad \sigma_t \le f_{ctm} \\ \\ f_{ctm}\cdot\left(\frac{\epsilon_{t,ck}}{\epsilon_t}\right)^{0.4} & for \quad \sigma_t > f_{ctm} \end{cases} \tag{2}$$

Additionally, account is made for the permanent reduction in elastic stiffness after crushing or cracking by use of a damage index, d_t or d_c for tension and compression respectively. These parameters are considered to be proportional to the maximum stress in each direction and vary from 0 for before the ultimate tensile or compressive stress is reached, up to 1 for a complete loss of stiffness (Simulia 2010).

For the concrete plastic model it requires the following inputs, the Dilation angle (ψ) was taken as 35°, an eccentricity (m) of 0.1, K_c factor of 2/3, ratio of initial equibiaxial compressive yield stress to initial uniaxial compressive yield stress (σ_{b0}/σ_{c0}) of 1.16 and a viscosity parameter of 0. These definitions and the values used come from the Abaqus user manual (Simulia 2010) and are all default values which convert the uniaxial stress strain relationship for compression and tension into the yield surface (Jankowiak and Lodygowski 2005).

The steel reinforcement was modelled with circular beam elements, element ID B31. The bond between the steel bars and the concrete was achieved by using Abaqus's embedded region feature, which constrains the translational degree between the elements nodes (Simulia 2010). Additionally, full bond was assumed between the steel and concrete, including along the entire anchorage length. Although this potentially overestimates the capacity provided by the steel in these regions, since no bar pull out was observed during the experimental validation tests, this simplification is considered adequate. Furthermore, as the Critical Shear Crack Theory, rather than FE results, was used for estimating shear strength, this approach is suitable for considering the response up to punching shear failure.

Solutions from nonlinear FE analysis are usually influenced by the mesh refinement. While a coarse mesh will not replicate the true stress gradients across a section, if there are localised areas of high tensile stress, decreasing the mesh size results in narrower crack bands and may not represent true distribution of stresses and strains. To determine a suitable mesh density, a mesh sensitivity study was conducted on the model for the corner removal with static loading condition (test C-S). It was found that using concrete elements 25mm wide by 6.67mm deep and 100mm rebar elements, which resulted in a model with 165312 elements requiring 264 hours of computational time, was a suitable balance between computational time and accuracy. In general, this refinement overestimates the deflections at the highest loading levels but it shows a good agreement within the elastic range and into the early cracking phase. For example, Table 1 compares the results of the mesh sensitivity analyses for the corner removal (test C-S). More information on about the mesh refinement can be found in Russell (2015). Figure 2 shows the meshed FE model. The bearing supports, as used in the experimental programme, can also be seen. These are fixed at their base but allow separation and rotation between the steel components.

Table 1. Results from mesh sensitivity study

		Coarse	Fine	Very Fine	Experimental
No. of concrete elements		27552	165312	344400	N/A
Slab Element Width (mm)		50	25	20	
Slab Element Depth (mm)		10	6.67	5	
Rebar Element Length (mm)		200	100	50	
Peak displacement at: (mm)	3.0kN/m^2	4.40	4.57	4.52	4.8
	6.0kN/m^2	15.00	18.44	18.01	15.1
	7.5kN/m^2	44.95	67.91	87.24	63.8
Computational Time (Hr)		28	264	431	N/A

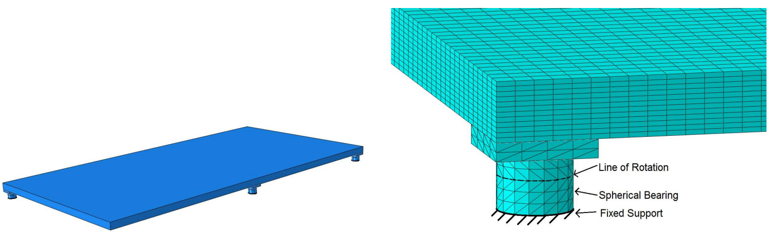

(a) Full model (b) Support and Boundary Condition

Figure 2. Rendering of the FE model showing mesh and boundary conditions

Validation against experimental results

Two static loading tests of RC flat slab substructures conducted by Russell et al. (2015) were replicated to validate the FE models. Both tests were based on a 2x1 bay 1/3 scale slab substructures as shown in Figure 3. Two column removal scenarios with uniformly distributed loads (UDLs) were considered, the loss of a corner (C) column and the loss of an edge column causing a penultimate (P) column loss (i.e. the bottom left and bottom middle columns in Figure 3 respectively). An FE model based on the geometry of the experimental slabs was constructed. Concrete and steel properties required for the material models were determined from tests conducted on samples taken during the experimental programme.

Support reactions were measured during the testing with load cells so comparisons could be made with the calculated values from the FE. The displacement readings recorded from LVDTs, were compared against nodal displacements at the equivalent positions. The locations of monitored points for displacements are shown in Figure 3.

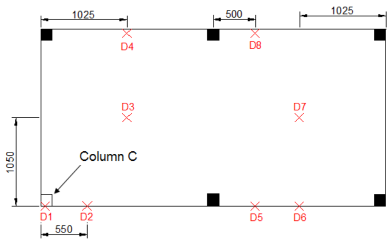

Figure 3. Locations of LVDTs and visual targets (D) from experiential programme for corner removal condition (Russell et al. 2015)

The final crack locations from the experiment were also compared to the plastic strain distributions in the concrete slab elements.

Force redistribution

The relative load on each support after a corner column removal case (test C-S) is shown in Figure 4. The solid lines show the FE results while the data points from the experimental test are also plotted to allow comparison. For all positions and for most of the loading, a very similar response is observed. There is a higher deviation at higher load levels (i.e. UDL $> 6\text{kN/m}^2$), with a maximum difference of 3.6 percentage points. This is due to the effects of cracking in the concrete, which reduces the stiffness around the supports. It should be mentioned that the proposed model does not capture this effect fully, partly because the plastic damage rule used leads to a gradual reduction in stiffness after cracking, whilst concrete often undergoes a sudden change. However, past the initial cracking phase there is again a strong agreement between the results and the overall response is considered to be good enough to make predictions on the demand placed on surrounding supports after a column loss.

Displacements

The force-displacement diagram is one of the key indicators into the suitability of the FE model as it allows validation of the elastic response of a structure and identifies the onset of cracking. It can also provide an indication of the ductility of the structure in the nonlinear range. As expected, at all recorded points there is an initial linear force-displacement response, however, once cracking starts to occur, there is a significant reduction in stiffness. Considering the displacement against loading for the corner

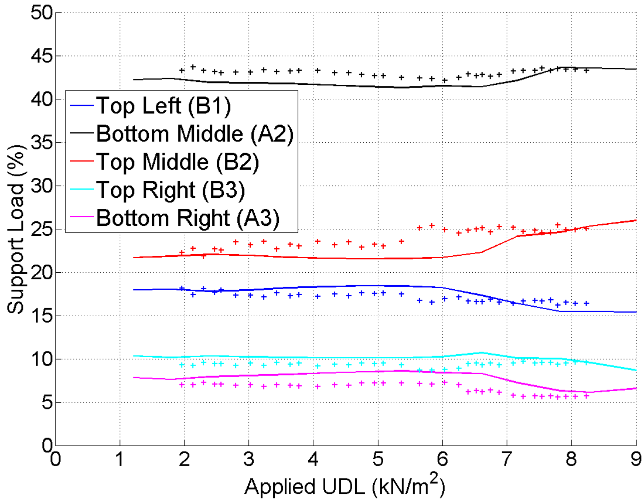

Figure 4. Distribution of forces to each support as loading increases. Test C-S. Solid line is FE model, +'s the experimental results

column loss condition shown in Figure 5, there is a very good agreement between the FE model and the experimental results. The locations of the monitored points were given in Figure 3. Both the positions presented match the initial stiffness of the experimental results at low levels of loading. After cracking occurs there was a sudden increase in displacements observed in the experimental case, however the FE model gives a more gradual response. This matches the tensile response of concrete described by Equation 2. Despite this effect, variation between the cases remains small for the whole range of load applied.

Flexural damage

It is important to consider the location and extent of damage when assessing the effect of a column loss on a structure. The finite element analysis gives an indication of the areas that might experience damage or cracking and these were compared with the cracking patterns from the experimental results.

The CDP model considers cracks to be a region of plastic deformation. Therefore, the location of the plastic strains should correspond to the location of cracks observed from the experimental case; this is compared in Figure 6. The location of cracks and plastic

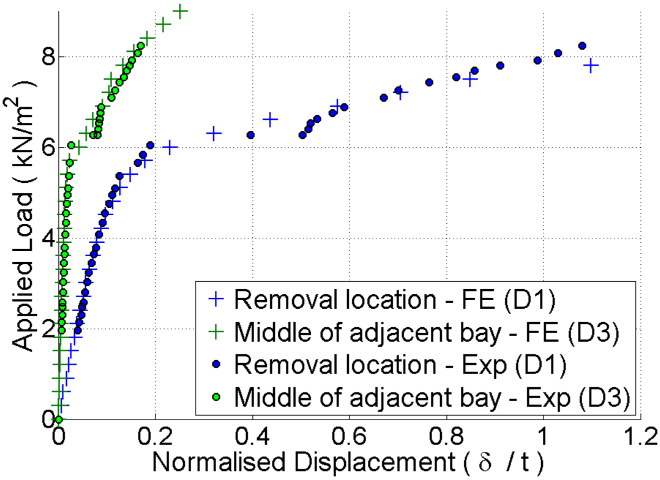

Figure 5. Normalised displacement against load for test comparing experimental results to the FE. Test C-S

strains (Figures 6(a) and 6(b) respectively) after a corner column loss, with 7.8kN/m^2 of loading is shown. The cracks and plastic strain follow the sagging yield lines acting between the supports and the damage occurs across most of the slab, with the most extensive effects close to the remaining corner support. In the adjacent bay the cracks can be seen to follow the reinforcement locations, which are also annotated, as was seen from the experimental results. On the top surface the cracks/plastic strains run between the supports with most of the damage concentrated in a fanning pattern of cracks around the middle supports (contrasting the radial pattern seen on the underside), which identifies the hogging yield lines resulting from the non-regular layout of remaining supports. All these patterns fit closely with the observed results discussed in more detail in the experimental work (Russell et al. 2015).

In general, the presented FE model correlates well to the results from the experimental slabs. In particular, the changes in reaction forces after a column loss show a close similarity, as do the locations of concrete cracks. This indicates that the stress distribution of FE model matches the true non-linear behaviour after a column loss scenario. The static displacements against load also correspond well between the experimental and FE cases, especially at the low loading levels. The higher loading conditions showed higher deviations due to the difficulty in defining the material properties for reinforced concrete

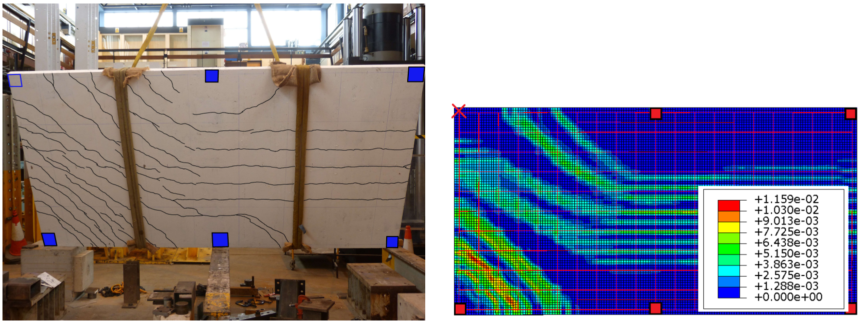

(a) Final crack locations from experiment (b) Equivalent plastic strain. Reinforcement is also annotated

Figure 6. Comparisons of bottom surface cracking patterns at 7.8kN/m^2 of loading for test C-S

Table 2. Values for the dimensions in Figure 7 used for the parameter study

Symbol	Label	Values (mm)
L	Span length	4000, 5000 and 6000
t	Slab thickness	180, 200, 250 and 300
L_{over}	Overhang	200
c	Column width	400
H	Storey height	3000

after extensive cracking has occurred for two-dimensional elements such as slabs. This leads to uncertainty in modelling the required nonlinear relationships for the extreme range. However, this occurs at higher deformations than is typical for accidental loading cases and so the proposed approach is considered suitable for the the range of conditions expected. Further information about the reference experimental tests and validation of the FE models can be found in Russell (2015).

Description of floor model

The validated FE model was extended to investigate the influence of changing different design parameters on the response of typical structures after a column loss event. A plan and elevation of the floor model is shown in Figure 7. Table 2 lists the geometric dimensions that were varied for the parameter study. The values used were limited by common configurations and the requirement to meet design guidelines.

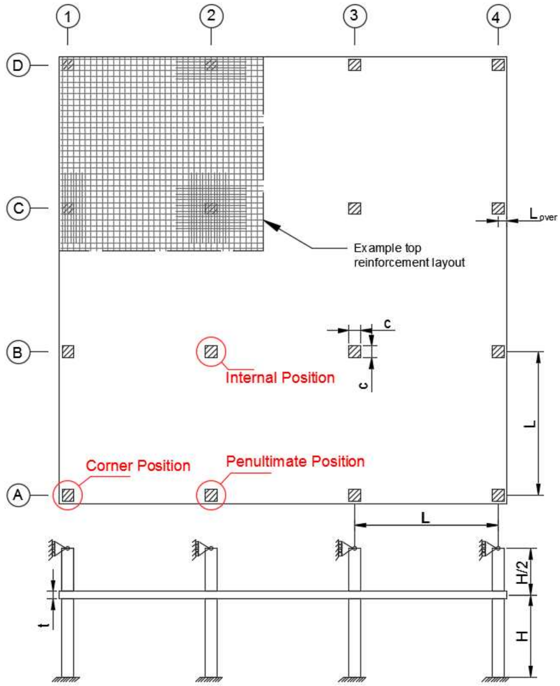

Figure 7. Plan and elevation showing labels, key column locations, typical reinforcement and grid markings

Each of the models was designed to meet current Eurocode requirements according to EN 1992 (2004). The structures were analysed using the equivalent frame method to obtain the required bending moments and shear forces. Characteristic dead loading was based on the selfweight of the material, taken as 25kN/m^3, plus an additional 1.0kN/m^2 to account for other finishes. Live loading for design was taken at 2.5kN/m^2. Unless otherwise stated, the characteristic compressive concrete strength was 30MPa. Based on the design forces, adequate flexural steel was provided, including the requirement to place 50% of the tensile steel for hogging moments within 0.125 times the span width. To meet durability specifications, 25mm of cover was provided to all steel. In all locations, for both top and bottom steel, at least a minimum area of steel was provided according to Eurocode requirements. Each model configuration met the required shear stress capacity without the inclusion of extra reinforcement. As the size of the columns was kept constant, the maximum span to depth ratio considered was limited by the shear capacity of the concrete.

Table 3. Span length and slab thickness for each model

Span length L (mm)	Slab thickness t (mm)	Effective span L_{eff}	Span to depth ratio L_{eff}/t
4000	180	3780	21.0
4000	200	3800	19.0
4000	250	3850	15.4
5000	200	4800	24.0
5000	250	4850	19.4
5000	300	4900	16.3
6000	250	5850	23.4

In total, seven different arrangements were considered as listed in Table 3. The span to depth ratios are based on the effective span length, L_{eff}, of an internal bay with a continuous slab over the supports according to Equation 3. These represent the range of span to depth ratios that are typical for flat slabs without shear reinforcement, i.e. 15–25.

$$L_{eff} = L - 2\left(\frac{c}{2}\right) + 2\left(\frac{t}{2}\right) \tag{3}$$

where the terms L, c and t are the span length, column width and slab thickness respectively, as identified in Figure 7 and Table 2. All bays were square and had the same span lengths, i.e. the aspect ratio of both the bays and the entire floor was constant.

Loading on the slab

For the FE simulations a UDL was applied to the entire slab area and was linearly increased up to the accidental load combination, w_{ac}, as given in Equation 4 from US General Services Administration (GSA) (2013), where DL and LL are the Dead and Live Loads respectively. While other load factors could be used to account for loading during an accidental event, this requirement is one of the highest commonly used.

$$w_{ac} = 1.2DL + 0.5LL \tag{4}$$

Once this level was reached, a further UDL was applied only to the bays around the lost column. The loading in this area was increased linearly up to a value of $2w_{ac}$, i.e. a Dynamic Amplification Factor (DAF) of 2.0. This additional load replicates the dynamic influence affecting those bays (Tsai and Lin 2009).

Punching shear calculations

Modelling of punching shear failure in finite element software is possible but requires the connections to be very carefully defined and the failure is more sensitive to mesh arrangement and the modelling solver. As has been demonstrated by others such as Genikomsou and Polak (2015), consideration of punching shear failure for a single connection is a demanding problem. For the size of floor slabs considered in this study, it would not be efficient to model the connections for this. Additionally, this work is focused on the response of the slab before punching shear failure and the potential complete collapse this could cause. As such, crack patterns, force redistributions, the displacement response and their relation to different column removal cases and geometric and material variables are not dependant on the shear approach used. Therefore each simulation was run to full loading and excluded shear failure and the punching shear capacity of the unreinforced flat slab connections was estimated with the Critical Shear Crack Theory (CSCT) developed by Muttoni (Muttoni 2008). The CSCT has been demonstrated to be suitable for assessing progressive collapse of flat slab structures (Micallef et al. 2014; Liu et al. 2015; Olmati et al. 2017) and the equation for predicting shear strength without transverse reinforcement is given in Equation 5, shown below,

$$\frac{V_R}{b_o d\sqrt{f_{ck}}} = \frac{3/4}{1 + 15\frac{\psi d}{d_{go}+d_g}} \tag{5}$$

where V_r is the shear force strength of the connection, b_o is the shear perimeter including a reduction to account of eccentric loading, d is the slab depth, f_{ck} is the concrete compressive strength, d_g is the aggregate diameter, ψ is the rotation of the slab, and is used as a proxy for crack width. The rotations and reactions were taken from the nonlinear finite element model which corresponds to a Level IV approximation from the Model Code 2010 (2012).

FE analysis results and discussion

Concrete cracking

During the analysis, cracking in the concrete elements was monitored to understand which areas of the structure were susceptible to flexural damage. The following results are based on the response of the model with a span to depth ratio of 19.4. However, it was seen that increasing the span to depth ratio primarily causes nonlinear behaviour due to cracking to occur earlier, but does not change the stress distribution and progression of

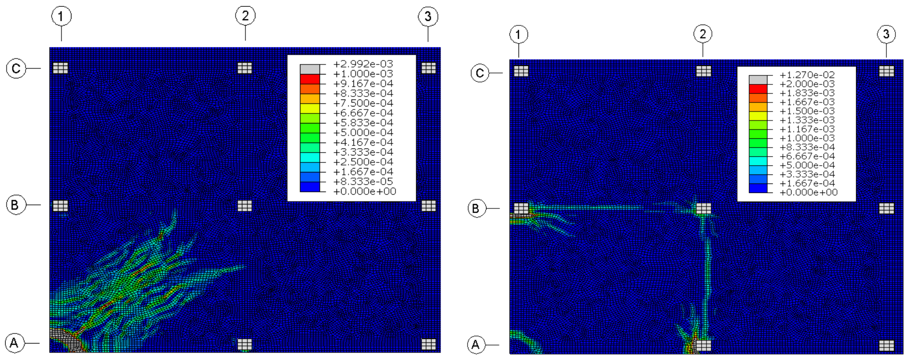

(a) Bottom surface cracks (b) Top surface cracks

Figure 8. Location of tensile plastic strain regions in the concrete elements after corner column (A1) removal; $w = 2w_{ac}$

damage patterns. Figure 8 shows the location and extent of plastic strains, representing cracks, that occurred after a corner column loss. Minimal plastic damage was observed before $1.5w_{ac}$. On the bottom surface (Figure 8(a)) diagonal cracks develop between the two orthogonally adjacent supports, as was observed during the experimental programme (Russell et al. 2015). However, these are limited to the bay directly around the removed column. On the top surface (Figure 8(b)) the cracks span between the surrounding supports, although the locations directly adjacent to the columns remain the most critical areas. Additionally, the start of a diagonal crack between columns A2 and B1 can be seen.

After an internal column removal, a similar response is observed with cracks concentrated directly next to the adjacent supports at relatively low loading (see Figure 9). By increasing the load, a large area of the structure is affected by extensive cracking on both the bottom surface (Figure 9(a)) and the top surface (Figure 9(b)). These plastic strains are larger, and cover more of the structure, than the corner condition, which explains why the internal column removal case has higher displacements, as shown later. It can also be noted that the hogging moments create cracks that surround the damaged bay and the sagging condition results in many cracks in the middle of the bay, however, the rest of the structure remains largely unaffected.

These cracking patterns demonstrate the change in stress distribution for a structure that has lost a column. For sagging moments, it is clear there is significant stress acting between diagonal columns (see B1-A2 for both presented cases). On the top surface the

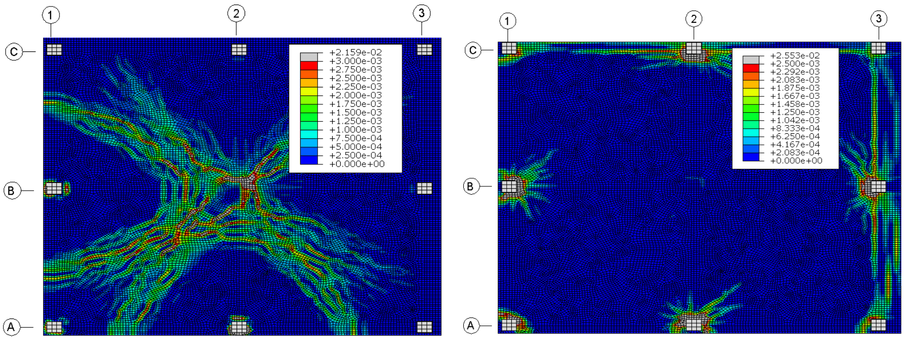

(a) Bottom surface cracks (b) Top surface cracks

Figure 9. Location of equivalent plastic strain regions in the concrete elements after internal column (B2) removal; $w = 2w_{ac}$

stress distribution has changed from the pattern expected for a regular column layout and now act perpendicular to grid line C1-C2 for internal case as well as towards the removed column location, perpendicular to line A2-B3, B3-C2 etc. The pattern of cracks match these seen in the experimental programme and the FE validation for the small slab section. In particular the radial yield lines around the remaining supports on the underside can be seen while on the top surface there is a fanning pattern around the adjacent supports after a column removal. Additionally, there is a clear hogging yield line acting between supports.

These concrete cracking patterns highlight the important changes to the internal forces in the slabs as a column loss event. For a flat slab with a regular arrangement of columns there is the traditional bending moment response along the grid lines. However, after a column removal event the span length will not be doubled, as would be predicted for a beam system, and a new bending moment arrangement forms utilising the shorter diagonal distance. Therefore the area around the removed column, although originally designed as a hogging moment location, may experience some sagging (particularly in an internal column removal case). The area of largest sagging bending stress is likely to be around the middle of the bay, which was designed for a sagging condition. However, the hogging bending stresses clearly extend to areas which were not intended for such conditions and may exceed their tensile capacity.

Understanding these effects is important for considering efficient changes to design for reducing damage after a column loss events.

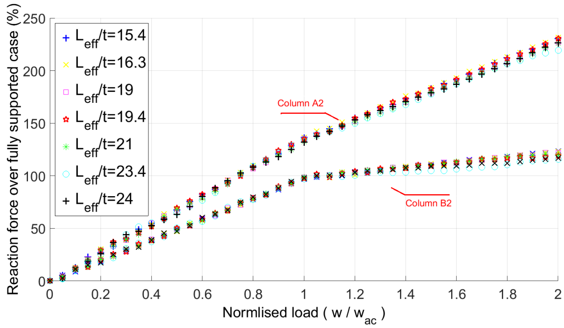

Figure 10. Change in column reaction forces due to static load increases for different span to depth ratios. Corner column removal

Reaction forces

Figure 10 shows the sum of reaction forces at two column bases as the static load is increased after a corner column loss. Column A2 is an orthogonally adjacent column to the removed location, see Figure 7, and experiences the highest increase in reaction force. For further comparison, column B2 is shown. The experimental programme indicated that this location (i.e. across the diagonal from the removed column) experienced a reduction in its relative loading (reaction force over fully supported case) as a result of the column loss. The seven models with different span to depth ratios are plotted and the reaction forces normalised against the fully supported condition with a load of w_{ac}. The main observation is that there is no significant difference in relative demand for structures with different span to depth ratios. As a result, all other comparisons will be made with just one configuration, L_{eff}/t=19.4. At a loading of $w = w_{ac}$ applied to the entire structure, column B2 exhibits a relative load of slightly less than 100%, demonstrating the demand is reduced. However, increasing the load in the critical bay results in a slight increase in loading at this location.

After a column loss, some of the remaining columns can experience a significantly higher load than they were previously carrying. This can be seen further in Figure 11, which shows the change in the column load, compared to its fully supported condition, for all the remaining columns after a corner (Figure 11(a)) or internal (Figure 11(b)) column loss. Due to the symmetry of the structure only half the columns are plotted. It can be seen from the results that the two orthogonally adjacent columns have the largest increase in vertical loading. As was observed during the experimental programme, there

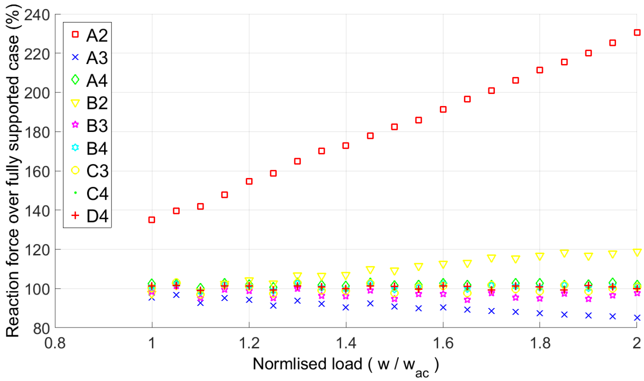

(a) Corner column removal (A1)

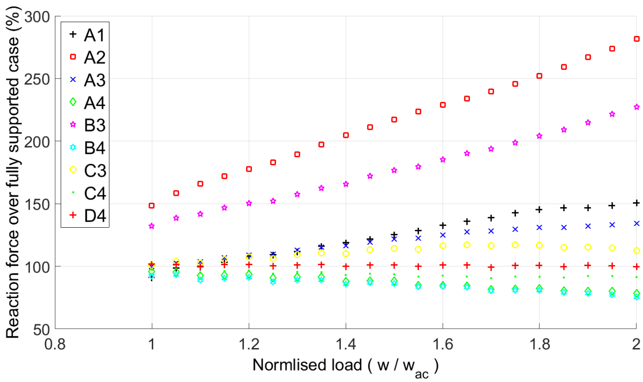

(b) Internal column removal (B2)

Figure 11. Change in column reaction forces due to static load increases. L_{eff}/t=19.4

is a linear increase in the loads transferred to each support, as total load is increased. However, it can be seen that at the higher loadings the effect of damage around the column changes this response as the slab is no longer truly continuous over the support and so force distributions change.

The highest relative increase in loading to a column for each scenario is given in Table 4. It is shown that, even without additional loading to account for dynamic effects, these locations were overloaded by at least 35%. As the load factor was increased to 2.0, critical columns are overloaded by up to 3 times their fully supported condition. Furthermore, although removing two columns could appear to be more critical scenario, as such an

Table 4. Summary of static reaction forces at remaining columns

Removed column(s)	Critical column(s)	Increase in reaction at: w_{ac}	$2w_{ac}$
Corner (A1)	A2/B1	135%	231%
Internal (B2)	A2/B1	148%	282%
Penultimate (A2)	A1	158%	301%
Two Column (A1 and A2)	A3	159%	251%

event influences a larger portion of the structure, the load can be redistributed to more columns and reduces the demand on a single location. This is seen in Table 4 where by the final loading, there is a larger maximum increase for Internal or Penultimate column removals than when two edge columns are removed.

Displacement response

In this study, to compare the effects of using different geometries, a displacement ductility factor μ_δ, is used as given in Equation 6

$$\mu_\delta = \frac{\delta}{\delta_y} \tag{6}$$

where δ and a δ_y are the displacement and the yield displacement of the removal point respectively. The yield displacement is obtained for each analysis by fitting a bilinear relationship to the response with the requirement to ensure the area under the simplified model is equal to the area under the measured curve. As δ/t (t=slab thickness) is also a common relationship in considering the relative magnitude of the deflections on the structure, both this ratio and the ductility factor will be used to discuss the response.

Figure 12 shows the corner displacement results for each span to depth ratio, normalised against the yield displacement. It is shown that there is a relationship between increasing the span to depth ratio and the ductility indicating more flexible slabs will exhibit more material nonlinearity within the loading range considered for design. Additionally, for configurations with a smaller L_{eff}/t, compressive membrane action can increase the stiffness of the slab reducing the damage and displacements Keyvani et al. (2014).

The displacement results of the corner removal case are presented in Table 5. The yield displacement varies between 0.013 and 0.067 times the slab depth. Up to the accidental load case, there are small displacements for all cases and usually a good linear trend is

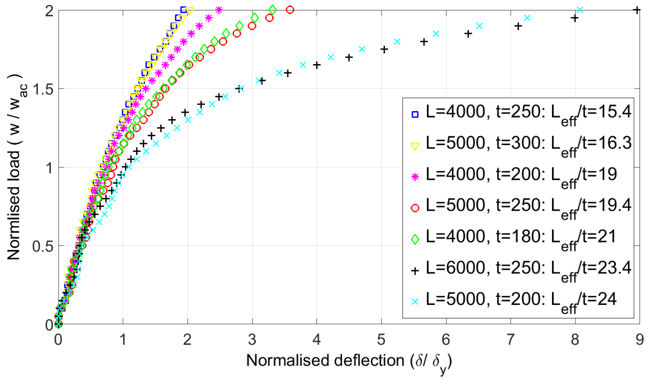

Figure 12. Displacement ductility factor, μ_δ, after corner column removal

observed, as displacements are usually less than δ_y. The coefficient of determination of a linear fit, R^2, values in Table 5 indicate that there has only been a minor reduction in the stiffness of the section due to the concrete cracking ($R^2 > 0.958$). As the load is increased further, displacements in the lower span to depth ratios remain small, while beyond a L_{eff}/t of 19.4 larger relative displacements, and associated damage occur.

For all cases, the nonlinearity in the displacement response starts when the increased bending moments generate cracking around the adjacent supports. There is then a gradual reduction in the stiffness as these cracks spread, as shown previously. During this phase, the underside of the concrete starts to crack, which further reduces the stiffness of the slab leading to larger deflections. This behaviour was more evident in flexible slabs with higher span to depth ratios.

As geometric nonlinearity, primarily due to the formation of a tensile membrane, typically only becomes significant beyond displacements of 0.5 times the slab depth, these results do not suggest this is a key factor. Additionally, it has been noted that in order for a tensile membrane to be effective, large rotations are required at the supports which may result punching shear failure before the secondary mechanism forms (Sagaseta et al. 2016).

A similar response is observed from an internal column loss, shown in Figure 13. In general, with a larger L_{eff}/t, greater normalised displacements occur. However, it can be seen that while L_{eff}/t=19.4 and 21.0 start off similar, by a loading of $2w_{ac}$ the theoretically stiffer model experiences higher relative displacements. The 19.4 case has a thicker section depth, 250mm compared to 180mm, and hence a higher self weight,

Table 5. Summary of static deflections - Corner removal

Span to depth ratio L_{eff}/t	Yield displacement δ_y/t	δ/t at w_{ac}	R^2 up to w_{ac}	δ/t at $2w_{ac}$
15.4	0.013	0.009	0.995	0.026
16.3	0.021	0.015	0.991	0.043
19.0	0.025	0.018	0.989	0.061
19.4	0.030	0.025	0.984	0.106
21.0	0.032	0.025	0.988	0.105
23.4	0.064	0.067	0.958	0.575
24.0	0.048	0.052	0.980	0.385

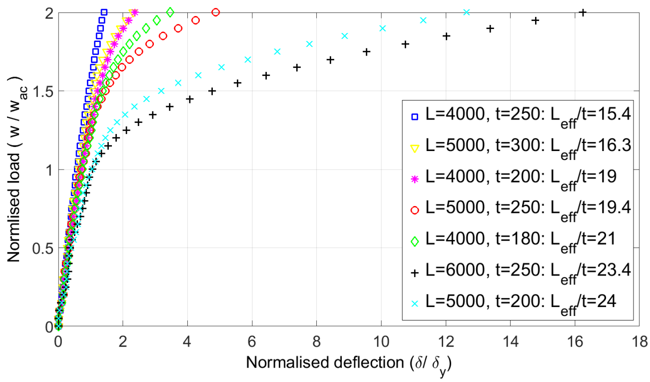

Figure 13. Displacement ductility factor, μ_δ, after internal column removal

which becomes more significant once concrete damage starts to occur. Considering all the configurations demonstrates that up to a loading of w_{ac} the system remains in the elastic range, however, once cracking starts to occur a significant nonlinearity is observed.

Of further interest is the response of other parts of the structure to a column loss. Figure 14 shows the normalised displacements against loading after the corner column has been removed for locations away from the removed column. From Figure 14(a) it is clear that the relative displacements in the bay adjacent to the one containing the removed column are very small especially for the stiffest structures. Figure 14(b) shows the results of locations further from the damaged area. As expected, all the models show a linear relationship up to w_{ac}. Beyond this point, load is only applied to the bay around the lost column, and therefore the adjacent bay and the middle bays show a slight uplift, while the furthest bay on the other side of the structure appears to be unaffected. Of final note is

Table 6. Load factor at first punching shear failure

Span (mm)	Thickness (mm)	Removal Location Corner	Internal	Penultimate	Two Column
4000	180	2.0+	2.0+		
	200	2.0+	2.0+		
	250	2.0+	2.0+		
5000	200	2.00	1.95	1.90	1.55
	250	2.0+	2.0+	2.0+	1.80
	300	2.0+	2.0+		
6000	250	1.70	1.55		

the response of the adjacent bay for the model with L_{eff}/t=21.0. At the highest loading level the pattern changes from an uplift to a slight downward trend. This is related to the damage sustained spreading into the adjacent bay and reducing its stiffness. Under other scenarios the same pattern was seen.

Punching shear assessment

For each scenario the connection rotations were calculated to obtain an estimate for the punching shear capacity at the remaining columns, according to Equation 5. Figures 15(a) and 15(b) give examples of the CSCT estimations for connection capacity. As can be seen for the L_{eff}/t=24.0 case, punching shear is predicted at the maximum level of rotation caused by the full DAF loading of 2.0, while with the longer span case, L_{eff}/t=23.4, punching shear occurs much earlier. Most other cases did not predict failure within the loading considered. Note that a lower concrete strength would naturally lead to an earlier punching shear failure.

The loading levels at which the first punching shear occurs after a corner or internal column removal is given in Table 6. It should be noted that if one connection fails, then failures at other columns are likely to occur leading to a progressive collapse. The majority of cases were loaded to the full DAF value of 2.0 without any failure occurring (therefore the failure load is designated as 2.0+, i.e. above the usual DAF), although the 6m span case was noticeably more susceptible. However, the other removal cases show that internal or penultimate column removals can result in shear failures at lower levels of loading.

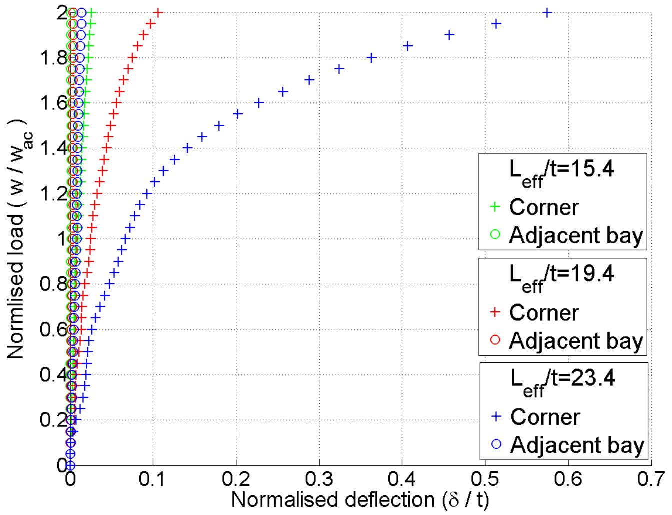

(a) Corner location and adjacent bay

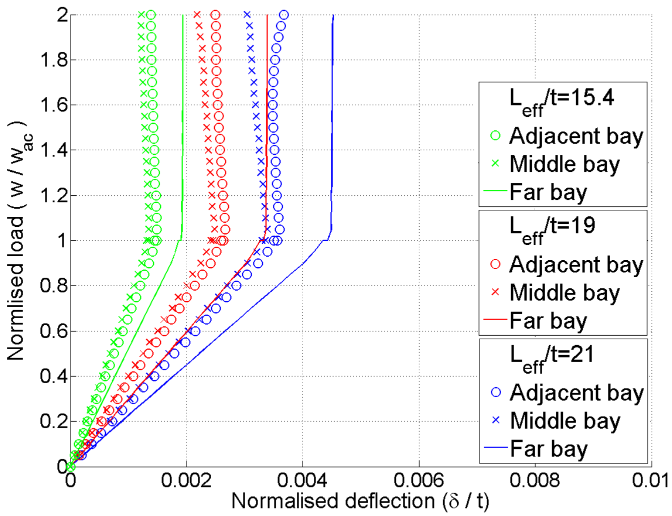

(b) Adjacent, middle and far bays

Figure 14. Normalised displacement at different locations against static loading. Corner column removed with different span to depth ratios

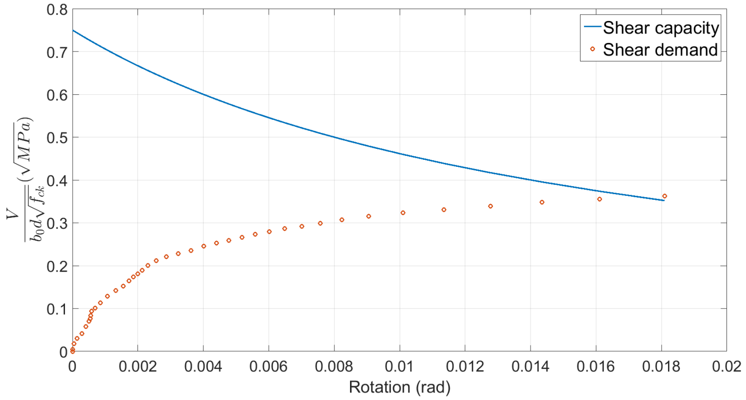

(a) L=5m, t=200, L_{eff}/t=24.0

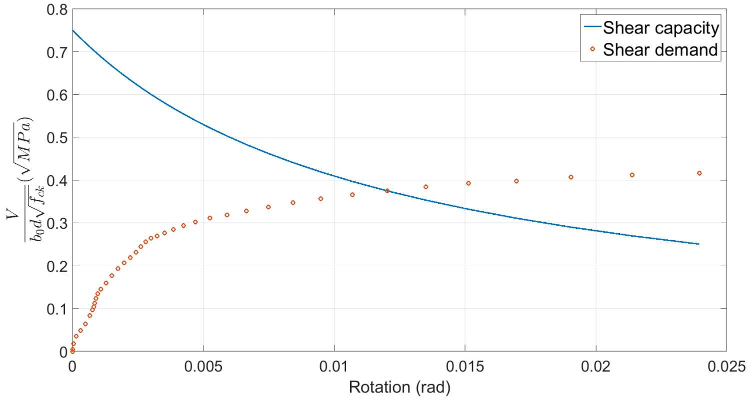

(b) L=6m, t=250, L_{eff}/t=23.4y

Figure 15. CSCT prediction of punching shear demand and capacity after a corner column removal.

Most critical removal locations

By comparing the maximum displacement for each removal condition, an indication into which situation is most critical can be determined. With L_{eff}/t=19.4 all the single column loss scenarios show a very similar response, as shown in Figure 16. At a loading of w_{ac}, the corner column loss shows the largest deformation by a small amount, however all three cases have very similar yield displacements, and remain within the elastic range.

Table 7. Displacement ductility, μ_δ, at different loadings for all column removal locations

Span to depth ratio, L_{eff}/t	Column location	$w = w_{ac}$	$w = 1.5w_{ac}$	$w = 2w_{ac}$
15.4	Corner	0.70	1.23	1.94
	Internal	0.58	0.94	1.41
19.4	Corner	0.86	1.65	3.59
	Internal	0.71	1.46	4.87
	Penultimate	0.75	1.52	4.11
	Two Columns	1.57	4.86	15.37
24.0	Corner	1.08	2.82	8.07
	Internal	1.02	3.18	12.64
	Penultimate	1.08	3.01	10.99
	Two Columns	1.50	5.59	16.68

By $2w_{ac}$ the loss of an internal column leads to the highest deflections compared to other removal cases, except for the stiffest case. Although these differences on the whole are not very large. Considering the case with L_{eff}/t=24, Figure 16 shows that the three cases have a very similar response at low loading levels, although by w_{ac} they have reached the yield displacement. Similar to the previous case, an internal column loss is the most critical scenario which becomes apparent after $1.5w_{ac}$.

For further comparison these values are also presented in Table 7. This highlights that for a single column loss, the displacement ductility demand increases by increasing the span to depth ratio, up to the accidental load case, w_{ac}, and all slab elements remain close to the elastic range. By a 50% increase in loading on the damaged bay, the displacements at the removal locations can increase up to 3 times the yield displacement. With a DAF of two, currently recommended for static analyses, the displacements exceeded 10 times the yield displacement, indicating a very strong nonlinear behaviour. The maximum ductility demands indicate that an internal column removal would be the most critical case for slabs with L_{eff}/t of 19.4 and 24, which is consistent with the displacement results presented before. However, corner column loss could lead to higher ductility demands in the slab elements with lower span to depth ratios (i.e. L_{eff}/t=15).

The loss of two columns, a corner and a penultimate edge, naturally creates a worse scenario with deflections higher than any of the other cases, and peak deflections more than four times the next largest value. This indicates that a structure that is considered safe against a single column loss could be vulnerable to progressive failures should a second column fail and if the structure does not have enough ductility to maintain its integrity.

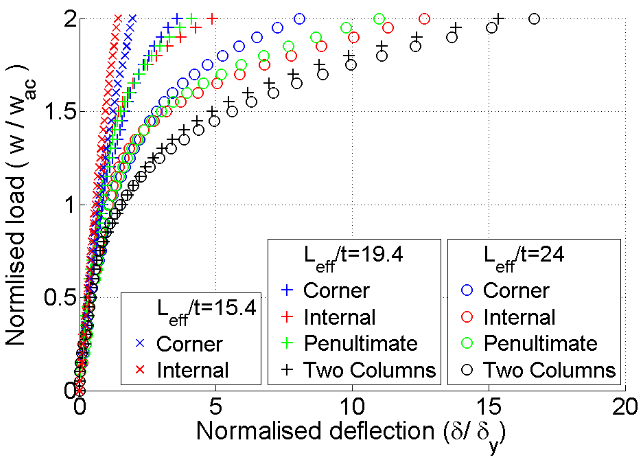

Figure 16. Normalised displacement against loading for different column loss scenarios

Effects of concrete strength

To investigate the effects of concrete strength on the behaviour of flat slabs after a column loss, a final comparison is made between three different compressive concrete strengths, based on displacement against loading curves, plotted in Figure 17. Two removal scenarios are presented for a model with L_{eff}/t=19.4. It is shown that up to w_{ac} there is very little difference in the response of the structures with different concrete strengths with displacements below, or close to, the yield displacement. Total variation between cases is less than 3mm for a slab with a depth of 250mm. However, as the loading is increased further, the lower strength concrete structure shows higher normalised displacements. Note that the lower concrete strength case had additional reinforcement to meet design requirements.

Of further note is the change in critical column loss scenario between corner and internal column removal cases. At all concrete strengths the corner loss causes a higher displacement at low loading levels. However, damage starts to occur at a lower load for the internal case which reduces its stiffness and causes higher final deflections. As the changeover point is dependent on the flexural damage to the slab elements, a higher concrete strength delays this effect.

A static analysis provides information on many of the important aspects for progressive collapse, and is commonly used for design. However, in reality, sudden column loss is a

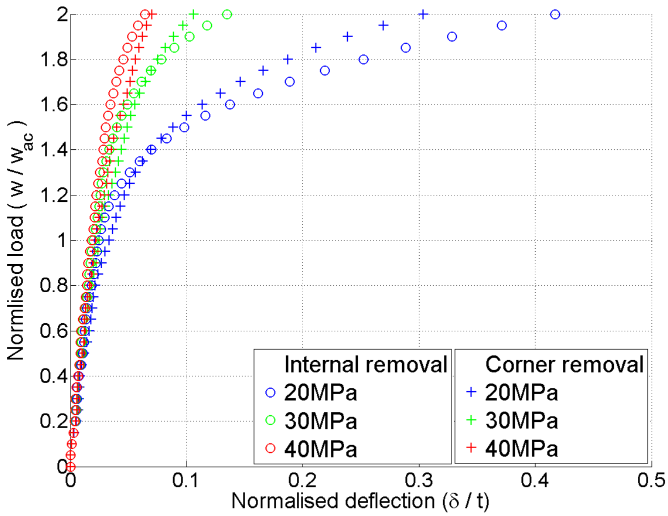

Figure 17. Normalised displacement against static loading for concrete strengths. Corner and internal column removal. L_{eff}/t=19.4

dynamic event that affects the demand placed on the structure due to inertial effects, and potentially increases the material strength if high strain rates are involved. The influence of the dynamic effects on flat slab structure will be addressed in a further paper.

Summary and conclusions

This study aimed to investigate the nonlinear behaviour of RC flat slab structures after a sudden column loss event. Non-linear finite element models were developed and validated against experimental results. It was shown that the models can accurately simulate the force-displacement response of the flat slabs and predict the location of concrete cracks and changes in the reaction forces after a column loss event. The validated FE models were then extended to investigate the effects of different design parameters such as span length, slab thickness and concrete compressive strength on the nonlinear response of flat slab structures considering different column loss scenarios. Based on the results presented in this paper, the following conclusions can be drawn:

- In general the flat slab systems showed to be robust and could redistribute the loads after a column loss by utilising alternative load paths. Changing the span to depth ratio did not affect the stress distribution and progression of damage patterns after a column loss. However, by increasing the span to depth ratio the nonlinear behaviour due to cracking occurred earlier.

- Beyond the elastic limits, damage and a permanent reduction in its stiffness occurred due to cracking of the concrete, with the most critical aspect being the extension of hogging bending stresses to areas that may not have been designed for such conditions. Compared to the corner column loss, an internal column removal affected a larger area of the slab and therefore led to higher displacement demands. Increasing the span to depth ratio (i.e. more flexible slabs) caused an increase in the displacement ductility demand after both corner and internal column. In general, the relative displacements in the bays adjacent to the one containing the removed column are very small especially for the stiff slabs with low span to depth ratios.
- There was no significant difference in the reaction force demands for structures with different span to depth ratios. After a corner or an internal column loss, the orthogonally adjacent columns to the removed location experienced the largest increase in their vertical loading (by up to 3 times after accounting for dynamic effects). It was shown that removing two columns simultaneously may not be the most critical design scenario as the vertical loads can be redistributed to more columns and reduce the demand on a single location.
- For long span slabs (over 5 m), the punching shear may occur at DAF values lower than the 2.0 suggested by the design guidelines. However, in shorter span slabs the punching shear was not usually a dominant failure mode. It was shown that, in general, the internal or penultimate column removals can result in shear failures at lower levels of loading.
- The results suggest that the most critical removal location depends on the slab geometry with an internal column removal case causing the largest nonlinear behaviour for stiffer slabs, and a corner column removal for more flexible slabs. Additionally, the use of low strength concrete results in structures more prone to progressive collapse, even after accounting for an increase in flexural reinforcement.

Acknowledgements

The authors would like to acknowledge the Early Career Research and Knowledge Transfer grant awarded by the University of Nottingham to Dr. Hajirasouliha that funded the project. They are also are grateful for access to the University of Nottingham High Performance Computing Facility, on which the simulations were run.

References

Eurocode 1992. BS EN 1992: Eurocode 2 - Design of concrete structures - Part 1-1: General rules and rules for buildings, 2004.

U. Cicekli, G. Z. Voyiadjis, and R. K. A. Al-Rub. A plasticity and anisotropic damage model for plain concrete. *International Journal of plasticity*, 23(10):1874–1900, 2007.

P. X. Dat and T. K. Hai. Membrane actions of RC slabs in mitigating progressive collapse of building structures. *Engineering Structures*, 55:107–115, 2013.

Fédération Internationale du Béton. *Model code 2010 : final draft*. Bulletin / Federation Internationale du Beton ; 65-66. International Federation for Structural Concrete (fib), 2012. Prepared by fib Special Activity Group 5, New Model Code.

D. M. V. Faria, V. J. G. Lucio, and A. P. Ramos. Post-punching behaviour of flat slabs strengthened with a new technique using post-tensioning. *Engineering Structures*, 40:383–397, 2012.

G. Flint, A. Usmani, S. Lamont, B. Lane, and J. Torero. Structural response of tall buildings to multiple floor fires. *Journal of Structural Engineering-ASCE*, 133(12):1719–1732, 2007.

Feng Fu. 3-d nonlinear dynamic progressive collapse analysis of multi-storey steel composite frame buildingsparametric study. *Engineering Structures*, 32(12):3974–3980, 2010.

N. J. Gardner, J. Huh, and L. Chung. Lessons from the Sampoong department store collapse. *Cement & Concrete Composites*, 24(6):523–529, 2002.

Aikaterini S Genikomsou and Maria Anna Polak. Finite element analysis of punching shear of concrete slabs using damaged plasticity model in abaqus. *Engineering Structures*, 98:38–48, 2015.

N. M. Hawkins and D. Mitchell. Progressive Collapse of Flat-Plate Structures. *Journal of the American Concrete Institute*, 76(7):775–808, 1979.

T. Jankowiak and T. Lodygowski. Identification of parameters of concrete damage pasticity constitutive model. *Foundations of Civil and Enviromental Engineering*, (6):53–69, 2005.

L. Keyvani, M. Sasani, and Y. Mirzaei. Compressive membrane action in progressive collapse resistance of RC flat plates. *Engineering Structures*, 59:554–564, 2014.

S. Kokot, A. Anthoine, P. Negro, and G. Solomos. Static and dynamic analysis of a reinforced concrete flat slab frame building for progressive collapse. *Engineering Structures*, 40:205–217, 2012.

Leslaw Kwasniewski. Nonlinear dynamic simulations of progressive collapse for a multistory building. *Engineering Structures*, 32(5):1223–1235, 2010.

J. H. Lee and G. L. Fenves. Plastic-damage model for cyclic loading of concrete structures. *Journal of Engineering Mechanics-ASCE*, 124(8):892–900, 1998.

J. Li and H. Hao. Numerical study of structural progressive collapse using substructure technique. *Engineering Structures*, 52:101–113, 2013.

J. Liu, Y. Tian, and S. L. Orton. Resistance of flat-plate buildings against progressive collapse. ii: system response. *Journal of Structural Engineering*, 141(12):04015054, 2015.

J. Lubliner, J. Oliver, S. Oller, and E. Onate. A Plastic-Damage Model for Concrete. *International Journal of Solids and Structures*, 25(3):299–326, 1989.

N. F. S. Mamede, A. P. Ramos, and D. M. V. Faria. Experimental and parametric 3D nonlinear finite element analysis on punching of flat slabs with orthogonal reinforcement. *Engineering Structures*, 48:442–457, 2013.

K Micallef, J Sagaseta, M Fernández Ruiz, and A Muttoni. Assessing punching shear failure in reinforced concrete flat slabs subjected to localised impact loading. *International Journal of Impact Engineering*, 71:17–33, 2014.

Y. Mirzaei and M. Sasani. Progressive collapse resistance of flat slabs: modeling post-punching behavior. *Computers and Concrete*, 12(3):351–375, 2013.

D. Mitchell and W. D. Cook. Preventing Progressive Collapse of Slab Structures. *Journal of Structural Engineering-ASCE*, 110(7):1513–1532, 1984.

A. Muttoni. Punching shear strength of reinforced concrete slabs without transverse reinforcement. *ACI Structural Journal*, 105(4):440–450, 2008.

H. Okamura and K. Maekawa. Nonlinear-Analysis and Constitutive Models of Reinforced-Concrete. *Computer Aided Analysis and Design of Concrete Structures, Vols 1 and 2*, pages 831–850, 1990.

P Olmati, J Sagaseta, D Cormie, and AEK Jones. Simplified reliability analysis of punching in reinforced concrete flat slab buildings under accidental actions. *Engineering Structures*, 130: 83–98, 2017.

T. W. Park. Inspection of collapse cause of Sampoong Department Store. *Forensic Science International*, 217(1-3):119–126, 2012.

A. T. Pham and K. H. Tan. Experimental study on dynamic responses of reinforced concrete frames under sudden column removal applying concentrated loading. *Engineering Structures*, 139:31 – 45, 2017.

K. Qian and B. Li. Slab Effects on Response of Reinforced Concrete Substructures after Loss of Corner Column. *ACI Structural Journal*, 109(6):845–855, 2012.

K. Qian and B. Li. Performance of Three-Dimensional Reinforced Concrete Beam-Column Substructures under Loss of a Corner Column Scenario. *Journal of Structural Engineering-ASCE*, 139(4):584–594, 2013.

M. F. Ruiz, Y. Mirzaei, and A. Muttoni. Post-Punching Behavior of Flat Slabs. *ACI Structural Journal*, 110(5):801–811, 2013.

J Russell. *Progressive collapse of reinforced concrete flat slab structures*. PhD thesis, University of Nottingham, 2015.

JM Russell, JS Owen, and I Hajirasouliha. Experimental investigation on the dynamic response of rc flat slabs after a sudden column loss. *Engineering Structures*, 99:28–41, 2015.

J. Sagaseta, N Ulaeto, and J Russell. Structural robustness of concrete flat slab structures. In *International Symposium on Punching Shear of Structural Concrete Slabs - Honoring Neil Hawkins (In fib bulletin 81)*, pages 273–298, 2016.

M. Sasani, M. Bazan, and S. Sagiroglu. Experimental and analytical progressive collapse evaluation of actual reinforced concrete structure. *ACI Structural Journal*, 104(6):731–739, 2007.

Simulia. ABAQUS Inc. User Manuel, version 6.10, 2010.

Y. P. Su, Y. Tian, and X. S. Song. Progressive Collapse Resistance of Axially-Restrained Frame Beams. *ACI Structural Journal*, 106(5):600–607, 2009.

N. Trivedi and R. K. Singh. Prediction of impact induced failure modes in reinforced concrete slabs through nonlinear transient dynamic finite element simulation. *Annals of Nuclear Energy*, 56: 109–121, 2013.

M. Tsai and B. Lin. Dynamic amplification factor for progressive collapse resistance analysis of an rc building. *The Structural Design of Tall and Special Buildings*, 18(5):539–557, 2009.

US General Services Administration (GSA). Alternate path analysis & design guidelines for progressive collapse resistance, 2013.

H. R. Valipour and S. J. Foster. Finite element modelling of reinforced concrete framed structures including catenary action. *Computers & structures*, 88(9):529–538, 2010.

R. Whittle. *Failures in concrete structures : case studies in reinforced and prestressed concrete*. CRC Press, 2013. Includes bibliographical references and index.

W. J. Yi, Q. F. He, Y. Xiao, and S. K. Kunnath. Experimental study on progressive collapse-resistant behavior of reinforced concrete frame structures. *ACI Structural Journal*, 105(4): 433–439, 2008.